Solar Energy Materials & Solar Cells 280 (2025) 113279

Contents lists available at ScienceDirect

Solar Energy Materials and Solar Cells

journal homepage: www.elsevier.com/locate/solmat

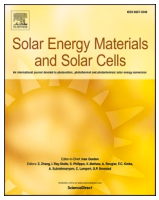

Sb_2S_3 solar cells with TiO_2 electron transporting layers synthesized by ALD and USP methods

T. Dedova [a,*], R. Krautmann [a], M. Rusu [b], A. Katerski [a], M. Krunks [a], T. Unold [b], N. Spalatu [a], A. Mere [a], J. Sydorenko [a], M. Sibiński [a], I. Oja Acik [a]

[a] Tallinn University of Technology, Department of Materials & Environmental Technology, Laboratory for Thin Film Energy Materials, Ehitajate Tee 5, EE-19086, Tallinn, Estonia

[b] Helmholtz-Zentrum Berlin für Materialien und Energie GmbH, Department Structure and Dynamics of Energy Materials, Lise-Meitner-Campus, Hahn-Meitner-Platz 1, 14109, Berlin, Germany

ARTICLE INFO

Keywords:
TiO_2 electron transport layer
Ultrasonic spray
Atomic layer deposition
Sb_2S_3 solar cells
USP
ALD
Kelvin probe
Photoemission spectroscopy

ABSTRACT

Electronic characteristics were investigated for solar cells (SCs) based on FTO/TiO_2/Sb_2S_3/P3HT/Au structure, employing TiO_2 electron transport layers (ETLs) fabricated by two different methods: ultrasonic spray pyrolysis (USP) and atomic layer deposition (ALD). Regardless of the deposition method, both ALD and USP-TiO_2 exhibit the anatase crystal structure. The calculated crystallite sizes, derived from the (101) reflection of TiO_2 layers using the Scherrer equation, show minimal variance between the two methods, with values 25 nm for USP and 30 nm for ALD TiO_2, respectively. Optical band gaps (E_g) were found to be 3.31 eV and 3.35 eV for USP and ALD methods, respectively. Exploring the thickness series of ALD-TiO_2, ranging from 100 to 1000 cycles (approximately 5–75 nm), solar cell performance was evaluated, with the highest power conversion efficiency (PCE) of 3.3 % achieved using ALD-TiO_2 of 400 cycles (approximately 30 nm thick). Notably, SCs featuring USP TiO_2 ETL layers, with a thickness of approximately 35–40 nm, outperform their ALD-TiO_2 counterparts, improving PCE by 15 %, recording 4.0 % versus 3.3 %, respectively. This superiority in PCE is attributed to the more favorable conduction band minimum (CBM) position of USP-TiO_2 relative to the Fermi level, as revealed in the band diagram. Specifically, a lower CBM spike at the USP-TiO_2/-Sb_2S_3 interface indicates reduced recombination rates compared to those at the ALD-TiO_2/-Sb_2S_3 interface. This study offers valuable insights into enhancing SC performance by optimizing deposition methods and synthesis parameters of ETL layers.

1. Introduction

In recent years, antimony chalcogenide compounds such as Sb_2S_3 [1–7], Sb_2Se_3 [8–11], and mixed chalcogenide $Sb_2(S,Se)_3$ [12–14] have been recognized by scientific community as promising alternative absorber materials to other popular thin film absorbers, such as CdTe and Cu(In,Ga)(S,Se)$_2$. High absorption coefficient ($>10^5$ cm^{-1}) in the visible range) [13,15], suitable tunable band gap, long carrier lifetime, decent carrier mobility, abundance, low toxicity, stability, theoretically high efficiency of 32 % [14] and thickness dependent semitransparency make antimony chalcogenide compounds an attractive absorbers for solar cells [1–8,10–16].

The less toxic and abundant sulfosalt materials are more preferable as an absorber layer in solar cells, compared to selenide ones [9,16] and therefore have been chosen for this study in spite of somewhat higher record efficiency of Sb_2Se_3 based solar cell compared to Sb_2S_3 based device, being 10.60 % and 7.08 %, respectively [1,12]. In order to improve the device performance, considerable efforts have been devoted to interface engineering and the development of an absorber layer [1].

Typical, Sb_2S_3 based solar cell, has a simple structure and composed of a front contact - glass substrate covered with conducting layer (FTO), electron transport material ETL (TiO_2), absorber layer (Sb_2S_3), hole, p-type conductor layer (HTL) and a back contact [2,3,17].

The main function of the ETL layer is to transfer the electrons to the external electrodes and blocking the backflow of holes at the same time [18]. A high-quality electron transport layer plays a key role in preventing charge recombination and rapidly extracts photoelectrons at the interface between the conducting substrate and the absorber active layer [19]. So far, the most widely used ETL layer for antimony chalcogenide binary absorber is CdS [13,15,20,21]. It has been shown that CdS has

* Corresponding author. author.
E-mail address: tatjana.dedova@taltech.ee (T. Dedova).

https://doi.org/10.1016/j.solmat.2024.113279
Received 31 May 2024; Received in revised form 4 November 2024; Accepted 4 November 2024
Available online 16 November 2024

excellent heterojunction band alignment with both Sb_2S_3 and Sb_2Se_3. Nevertheless, it exhibits a low band gap energy (E_g) of 2.4 eV, which leads to significant optical losses in CdS/Sb_2S_3 via parasitic absorption in the short wavelength region. Furthermore, chemical intermixing has been reported between CdS and Sb_2Se_3 at elevated processing temperatures, which is thought to introduce a CdSe interface layer that acts as an electrostatic barrier to electron transport [22,23]. Alternative to CdS junction partners are ZnO, SnO_2 and TiO_2. Among those, TiO_2 is a suitable ETL combining advantages of high stability, and wide band gap [23,24]. Due to the band gap of above 3 eV, TiO_2 can efficiently reduce the parasitic absorption associated with current losses, enhancing the short circuit current of a solar cell [25,26]. So far, TiO_2 has demonstrated the highest efficiency in solar cell devices, compared to ZnO or SnO_2 ETLs [1,21]. The device with structure FTO/TiO_2/Sb_2S_3/Spiro-OmeTAD/Au has gained a record efficiency of 6.8 %, based on spin-coated TiO_2 ETL layer [1]. Solution based methods, such as spray pyrolysis, sol-gel, spin coating, hydrothermal growth are the most widely used methods for the deposition of TiO_2 as ETL layer for various types of solar cells [1–3,25–29]. As a rule, solution based grown TiO_2 exhibit either anatase or a mixture of amorphous and anatase phases. A phase modification to more stable rutile TiO_2 usually requires post deposition annealing temperatures over 600 °C [30,31]. It is well known that various ways of synthesis affect the films properties including the morphology, crystallinity and optoelectronical properties that, in turn, affect the properties of subsequent layers deposited on top of the firstly synthesized, prior layers [32–34]. So far, ALD method for deposition of TiO_2 as ETL layer is the most widely used in perovskite type solar cells [35–41]. Among the methods employed to obtain TiO_2 films, ALD method is proven, highly precise, reproducible, allow to get uniform, high quality, dense TiO_2 coverage [42–44]. It was reported in the literature, that thickness of ALD grown TiO_2 film largely alters the solar cell performance, however, optimal thickness of TiO_2 giving highest perovskite type SC output parameters varies from 2 to 200 nm from paper to paper [38]. Therefore, the thickness of the TiO_2 layer should be always optimized for every new solar cell configuration and therefore various thicknesses of ETL layers were tested in this study. Alternatively, to ALD, there are also other attractive methods to deposit TiO_2 thin films. Namely, spray pyrolysis is another convenient choice to prepare not only the TiO_2 layer, but also Sb_2S_3 absorber layer [2,3,6]. Employment of spray pyrolysis shows a growing interest among researchers due to cost-effectiveness, simplicity of the apparatus and ability to deposit main solar cell component layers sequentially in less than 1 h [2,3,45]. Since the various ways of synthesis may affect the films properties such as morphology, crystallinity and optoelectronic properties [32–34] the comparative studies that include multiple preparation methods of the layers in a single study often provide a better understanding on the specific characteristics, growth and formation of the targeted layer dependent on the underneath layer property. So far, the publications on Sb_2S_3 solar cells are mainly focused on the optimization of an absorber, Sb_2S_3 layer [3,35,40], and HTL layer [2,9] rather than on ETL layer [2,3,6,35,40]. However, the comparative studies that would employ different synthesis methods of the solar cell components are missing in the literature. In spite of TiO_2 plays a paramount role in this type of a solar cell structure and ALD method is one of the most attractive deposition methods, there are no studies found so far focused on ALD deposited TiO_2 films incorporated into Sb_2S_3 solar cell.

In this paper we provide a systematic comparative study on ALD and USP deposited TiO_2 layer performance, as an ETL component of a solar cell with glass/FTO/TiO_2/Sb_2S_3/HTL/Au configuration. We study the influence of different thicknesses of ALD deposited TiO_2 on SC device performance and compare those with spray pyrolysis deposited TiO_2 ETL layer with fixed and previously optimized thickness [3]. We study the morphological, structural and optical properties of the obtained TiO_2 films by means of SEM, XRD and UV–VIS spectroscopy techniques. We explore the effect of ETL TiO_2 layer grown by USP and ALD methods on the structural properties of grown on them Sb_2S_3 absorber layer. The output parameters of the complete solar cells by means of current-voltage (J-V) characteristics. Finally, we compose and compare band diagrams of solar cells based on ETL layers prepared by USP and ALD methods using data of Kelvin probe (KP) and Photoelectron Yield Spectroscopy (PYS) measurements of all the cell component layers to get deeper insight into the solar cell behaviour. On this basis we draw the conclusions according to the optimal cell production process parameters.

2. Experimental

2.1. TiO_2 layers deposition and SC preparation

First, 1.2 mm thick glass/FTO substrates (Alfa Aesar) covered by 300 nm thick and 7 Ω/square resistivity FTO layer were used as substrates to grow TiO_2 films. Those conductive layers were cleaned with a detergent solution, isopropanol and subsequently washed with double deionized water prior the deposition of TiO_2. Next, additionally, to a wet cleaning procedure, substrates were treated under UV-C light illumination for 30 min.

Then, TiO_2 ETL layers were deposited by two techniques, either by an ultrasonic spray pyrolysis (USP TiO_2) or an atomic layer deposition method (ALD TiO_2). The USP TiO_2 films were grown by spraying the solution mixture of 0.1 mol/L titanium tetraisopropoxide (TTIP) and 0.4 mol/L acetylacetone dissolved in ethanol. USP TiO_2 ETL was deposited spraying 75 cycles (35–40 nm thickness). This USP TiO_2 fabrication route is chosen based on research group previous intensive studies on Sb_2S_3 solar cell technological optimization applied for USP TiO_2 and the whole solar cell stack deposition [2,3,6]. Thus, the USP TiO_2 films thickness is kept unchanged through this study. The films were deposited at 340 °C in air atmosphere and annealed at 450 °C for 60 min in air.

ALD-TiO_2 have been deposited by ALD deposition system, model R-200, PICOSAN. $TiCl_4$ and deionized (DE) water were used as precursors for the deposition. The substrate temperature was set to 125 °C. Volumetric flow rate of $TiCl_4$ was 150 sccm, 0.1 s pulsing and 3 s purging time. Volumetric flow rate of DE water was 200 sccm, 0.1 s pulsing and 4 s purging time. The thickness of the resultant TiO_2 layers was adjusted through the number of pulses and additionally controlled by SEM cross sectional images of the complete solar cell structure. The number of pulses were 100, 200, 400, 800 and 1000 cycles corresponding to ca. 5, 15, 30, 60 and 75 nm (Proved by SEM cross-section images, not presented here). After the deposition of TiO_2 by ALD, the films were annealed in air at 450 °C. To preserve the access to the back contact, the 3 mm wide stripe of heat resistant Kapton® tape was temporarily glued onto a FTO side prior the deposition of TiO_2 layers.

In order to study the structural properties, phase composition and optical properties of TiO_2 ETL layers separately, TiO_2 layers were deposited on FTO/glass and glass substrates applying 400 cycles for ALD and 70 cycles for USP-TiO_2. To keep the synthesis conditions similar to those used in solar cells, the ALD-TiO_2 films undergone the annealing procedure in air at 450 °C.

Further, the absorber layer, Sb_2S_3, has been deposited by ultrasonic spray pyrolysis from a mixture of 0.1 mol/L $SbCl_3$ and 0.3 mol/L thiourea (molar ratio of 1:3) at 200 °C with a nebulization frequency of 1.7 MHz and a power of 200 W.

Polythiophene, P3HT, was used as a hole conductor material and was deposited by spin coating technique on a top of Sb_2S_3 layer. Finally, gold contacts were deposited by vacuum evaporation.

Experimental details on Sb_2S_3 and P3HT depositions can be found in earlier papers [3,6].

2.2. Characterization

A Zeiss HR FESEM was used to examine the surface and cross-sectional morphologies of the layers. The total transmittance and total reflectance spectra of Glass/FTO/TiO_2 samples were recorded using a

Jasco V-670 ultraviolet–visible spectrophotometer (UV–VIS) in the range of 300–1000 nm. Glass/FTO substrate was used as reference for total transmittance measurements. The absorption coefficient, α, was calculated by the equation [46]:

$$\alpha = -\frac{1}{d}\ln\left[\left(\left((1-R)^4 + 4T^2R^2\right)^{\frac{1}{2}} - (1-R)^2\right)\Big/ 2TR^2\right], \quad (1)$$

where d is the film thickness, R is reflectance and T is transmittance. Tauc' plot model [47,48] was used to determine the band gaps of TiO_2 assuming indirect band transition.

The phase composition and structure were characterized by X-ray diffraction (Rigaku Ultima IV, Si strip detector D/teX Ultra, 0–20, CuKα$_1$, λ = 1.5406 Å, 40 kV, 40 mA, 5° min^{-1}, step 0,02°). A texture coefficient (TC) of main crystal planes of Sb_2S_3 were calculated from equation (2)

$$TC(hkl) = \frac{I(hkl)}{I_0(hkl)} \times \left[\frac{1}{N}\sum_{i=0}^{N}\frac{I(hkl)}{I_0(hkl)}\right]^{-1} \quad (2)$$

where I(hkl) is the measured intensity of a (hkl) crystal plane, I_0(hkl) is a reference intensity of the respective crystal plane obtained from the JCPDS Card No. 42–1393, and N is the number of crystal planes included in the analysis.

Work function (Φ), ionization energy (E_i) and the energy difference between Fermi level (E_F) and valence band maximum (E_{VBM}) of the TiO_2 films were measured by Photoelectron Yield Spectroscopy (PYS) and Kelvin Probe (KP) techniques at atmospheric pressure under N_2 ambient by a KP Technology SKP5050-APS02 instrument [49]. The setup was placed in a Faraday cage to shield external electric fields and enable controlled illumination of the sample. The samples were contacted with carbon tape and mounted on a motorized 3-axis stage with a precision of less than 300 nm. The top counter electrode was a 2.0 mm diameter electrode with a gold-alloy coating.

KP was performed with the vibrating top reference electrode, i.e. Kelvin probe, with a work function, Φ_{tip}, calibrated against a gold reference sample. The work function of the sample, Φ_{sample}, was determined according to $\Phi_{sample} = \Phi_{tip} + e{\cdot}CPD$ where e is the elementary charge and CPD is the contact potential difference between the Kelvin tip and the investigated sample. The CPD was measured with a resolution of 1–3 mV. The measurements of the surface photovoltage (SPV) defined as $SPV = CPD_{light} - CPD_{dark}$ were performed using laser diodes with wavelength/energy of 405 nm/3.06 eV, 450 nm/2.75 eV, 532 nm/2.33 eV, and 670 nm/1.85 eV with a light power density of ≈100 mW/cm^2. As can be seen, the SPV can be also determined as $SPV = \Phi_{light} - \Phi_{dark}$. The SPV sign is used for determination of the conductivity type of the measured materials. Due to different types of surface termination and defects, a *p*-type material shows usually a downward band bending at the surface and thus $\Phi_{light} > \Phi_{dark}$, resulting in SPV >0 (see detailed band diagrams in Supporting Information to Ref. 49). An SPV >0 points in addition to separation of electrons to the measured surface, as driven by the downward bending of the bands. Similar considerations for an *n*-type material led to an SPV <0 and separation of holes to the measured surface. Thus, when investigating solar cell device stacks, the SPV sign proves the type of charge carriers which separate to the surface adjacent to the Kelvin tip.

PYS measurements were performed by using the same Kelvin tip in static regime at a tip-sample distance of less than 1 mm. A bias voltage of 10 V was applied between the sample and the electrode to collect the charges. The sample was illuminated by a deuterium light source coupled with a grating monochromator, providing excitation from 3.4 to 7.6 eV. Measurements were conducted with a step of 1 nm and the photoemission threshold was determined with a resolution of 30 meV. The light was guided by a DUV optical fiber and focused on the sample with an elliptical spot of ≈2 × 3 mm^2. Further details on the KP-PYS setup and data evaluation can be found elsewhere [49].

The current–voltage (*I–V*) characteristics of the fabricated solar cells were recorded with a Metrohm Autolab potentiostat PGSTAT302N at room temperature. For the measurements under illumination, factory calibrated solar simulator Wavelabs LS-2 LED was applied with the light source corresponding to the AM1.5G (100 mW cm^{-2}).

3. Results and discussion

3.1. Structural and optical properties of ALD and USP TiO_2 layers

XRD patterns of annealed ALD and USP-TiO_2 layers deposited on FTO/glass substrates are presented in Fig. 1a. The reflections at 2 theta of 25.4° and 48.3° correspond to (101) and (200) planes of anatase TiO_2 crystalline phase, are present in both XRD patterns of ALD and USP deposited TiO_2 thin films [50]. No diffraction peaks related to rutile or brookite crystal phases of TiO_2 were detected, further indicating the presence of anatase phase only. That is in good correspondence with earlier studies on USP [51,52] and ALD deposited TiO_2 [53,54]. As can be seen on Fig. 1a, the XRD patterns are dominated by the FTO substrate. TiO_2 films were deposited also onto glass substrates and the results are presented in SI on Fig. S1. As could be seen that amorphous TiO_2 is present in as-deposited stage, and the formation of anatase phase occurs after annealing the films at 450 °C. Thus, we can conclude here, that anatase TiO_2 film is formed by ALD an USP methods after annealing, irrespective of the applied deposition method.

The crystallite sizes, calculated by Scherrer equation from the full width at half maximum (HWHM) of (101) crystal plane, are close in values independent of the deposition method used, being 25 and 30 nm for USP and ALD TiO_2, respectively.

The total transmittance and reflectance spectra of ALD and USP deposited TiO_2 films are presented as Figs. S2in SI. The total transmittance of the TiO_2 films is ca 65 % in the visible spectral range, and the reflectance remains ca 10 %.

Tauc plot method was used to determine the E_g of TiO_2 films, which were found by XRD to crystallise in the anatase phase. Since the anatase TiO_2 is an indirect band gap (E_g) semiconductor [55,56], the band gaps were determined from $(\alpha h\nu)^{0.5}$ plots as function of photon energy. As seen in Fig. 1b, two segments (slope 1 and 2) can be observed on both ALD and USP-TiO_2 graphs that can provide a linear fitting, indicating two different optical transitions, both assigned to indirect transitions in the anatase TiO_2 indirect band gap. The slope 1, at higher photon energies, is associated with transition assisted with phonon emission, while the linear part in the lower energy range, slope 2, is associated with transitions assisted by phonon absorption [57]. The intercepts of linear part of slope 1 to x-axis gave values of 3.42 and 3.47 eV, and slope 2 of 3.20 and 3.22 eV for USP and ALD-TiO_2, respectively, as shown in Fig. 1b. Based on the intercepts of those two slopes, we calculate the so-called medium value for the indirect band gap. The optical E_g values equal to 3.31 eV and 3.35 eV for USP and ALD-TiO_2, respectively. Such approach is usually applied for single crystalline materials [58,59]. However, some reports showed its applicability for polycrystalline thin films too [47,48]. The obtained E_g values for TiO_2 are consistent with values reported in previous studies, where the E_g values for anatase TiO_2 have ranged from 3.20 to 3.40 eV as extracted based on Tauc plots [53,60,61] as well as from the slope of the Kelvin probe contact potential difference spectra [62].

The cross-sectional HR-SEM images of FTO/TiO_2/Sb_2S_3/HTM/Au stack with USP and ALD-TiO_2 ETLs in solar cell structure are presented in Fig. 2a and b, respectively. The thickness of USP-TiO_2 is in the range of ca. 35–40 nm, and ALD is about 30 nm for the samples obtained from 400 cycles. As can be seen from the figure, the dense and uniform TiO_2 is formed independently of the deposition method. The morphology of USP deposited TiO_2 seems to be grainy, whereas the morphology of ALD TiO_2 layer looks smooth.

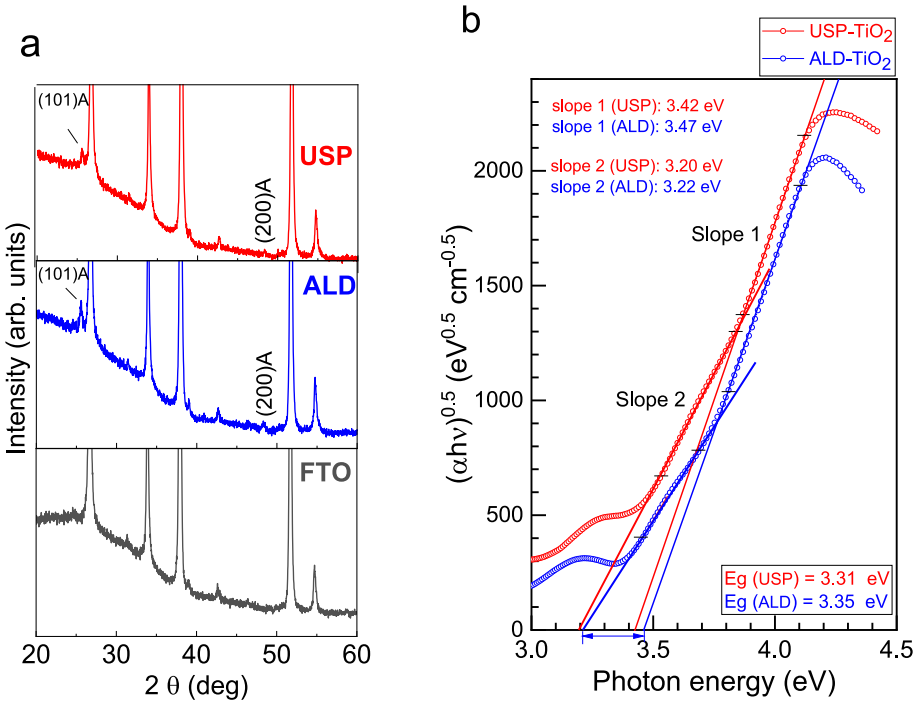

Fig. 1. a) XRD patterns of glass/FTO substrate, ALD TiO_2 (400 ALD cycles) and USP TiO_2 (70 spraying cycles) films deposited on glass/FTO substrates. b) Tauc's plots after subtraction of the baselines for E_g evaluation of the ALD and USP-TiO_2 ETL layers deposited on glass/FTO substrates. The calculations use the UV–VIS total transmittance spectra measured using glass/FTO substrates as a reference.

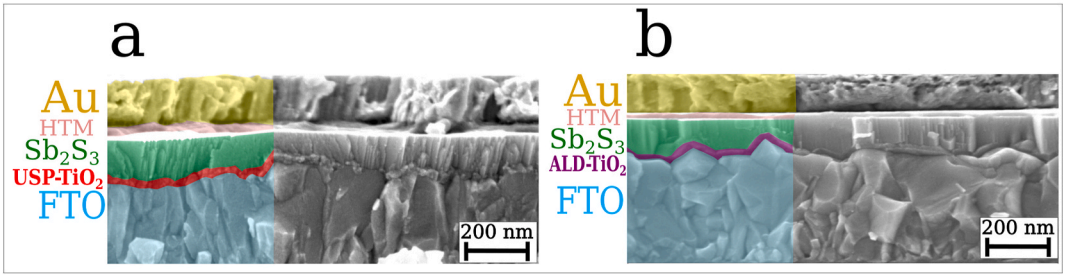

Fig. 2. HR- SEM cross-sectional images of FTO/TiO_2/Sb_2S_3/HTM/Au SC stack with a) USP TiO_2 (75 spraying cycles, corresponding to TiO_2 film with a thickness of 35–40 nm) and b) ALD TiO_2 (400 cycles corresponding to TiO_2 film thickness of 30 nm).

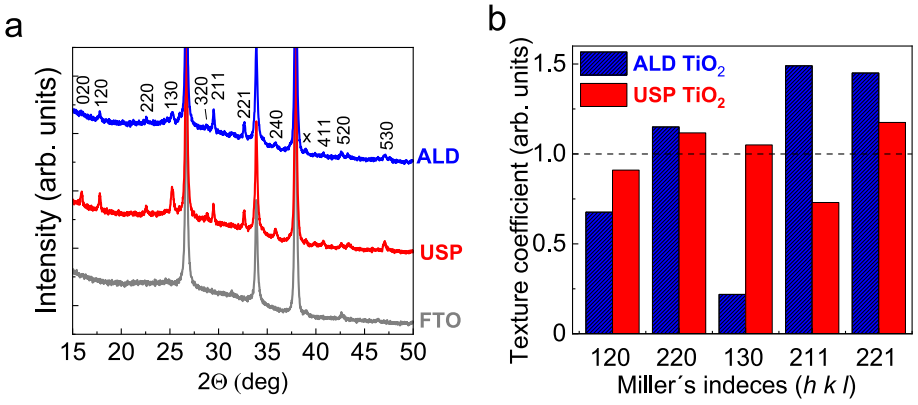

Fig. 3. a) XRD patterns of FTO/TiO_2/Sb_2S_3 structures with Sb_2S_3 layers grown on either USP or ALD TiO_2 layer. (hkl) correspond to Sb_2S_3, x corresponds to TiO_2 b) Texture coefficient values for respective crystal planes of Sb_2S_3.

3.2. Impact of TiO_2 ETL on the growth and texture of Sb_2S_3 absorber deposited by USP

Structural properties of Sb_2S_3 films were studied by XRD and texture coefficient (TC) analysis, which could help determine how the ETL TiO_2 film growth method has affected the Sb_2S_3 film growth. XRD patterns of glass/FTO/TiO_2/Sb_2S_3 structures, with both ALD- and USP-fabricated TiO_2, are shown in Fig. 3a. Regardless of the deposition method used to fabricate TiO_2 films, both ETL layers facilitate orthorhombic crystal growth of Sb_2S_3, with reflections at 2 theta of 17.5°, 22.3°, 24.9°, 29.3° and 32.4° corresponding to the (120), (220), (130), (211) and (221) crystallographic planes, respectively.

TC analysis for main crystal planes of Sb_2S_3, as shown in Fig. 3b, indicates that different ETL films grown either by ALD or USP method can impact the Sb_2S_3 absorber crystal growth and orientation. Sb_2S_3 film deposited onto ALD-TiO_2 show slight increase of TC values for (211) and (221) planes. In addition, its TC value for (130) plane is five times lower compared to the TC of Sb_2S_3 grown onto USP-TiO_2 layer. Facilitating grain growth of (hk1) Sb_2S_3 crystals, while limiting growth of horizontally oriented (hk0) planes, is a growth strategy multiple research groups have adopted to improve carrier properties of Sb_2S_3 solar cells [20]. It follows the theory, which states that crystals oriented more toward the normal of the plane allow electrons to move more freely across the absorber layer into the ETL. Comparing the crystal growth of the two TiO_2 films, the TC values suggest that there is a greater presence of favorable (hkl) planes in TiO_2 deposited by ALD method.

3.3. Effect of TiO_2 ETL on solar cell device performance

The output parameters of solar cells (SCs) employing TiO_2 layers fabricated by ALD and USP methods are demonstrated in Fig. 4 and Table 1.

Analysis of the data reveals a significant impact of ALD-TiO_2 layer thickness on solar cell output parameters. SCs with thin ALD-TiO_2 ETL layers (approximately 5 nm, 100 cycles) exhibit comparatively weak output parameters, with average PCE of 1.8 %, respectively. Low V_{OC}

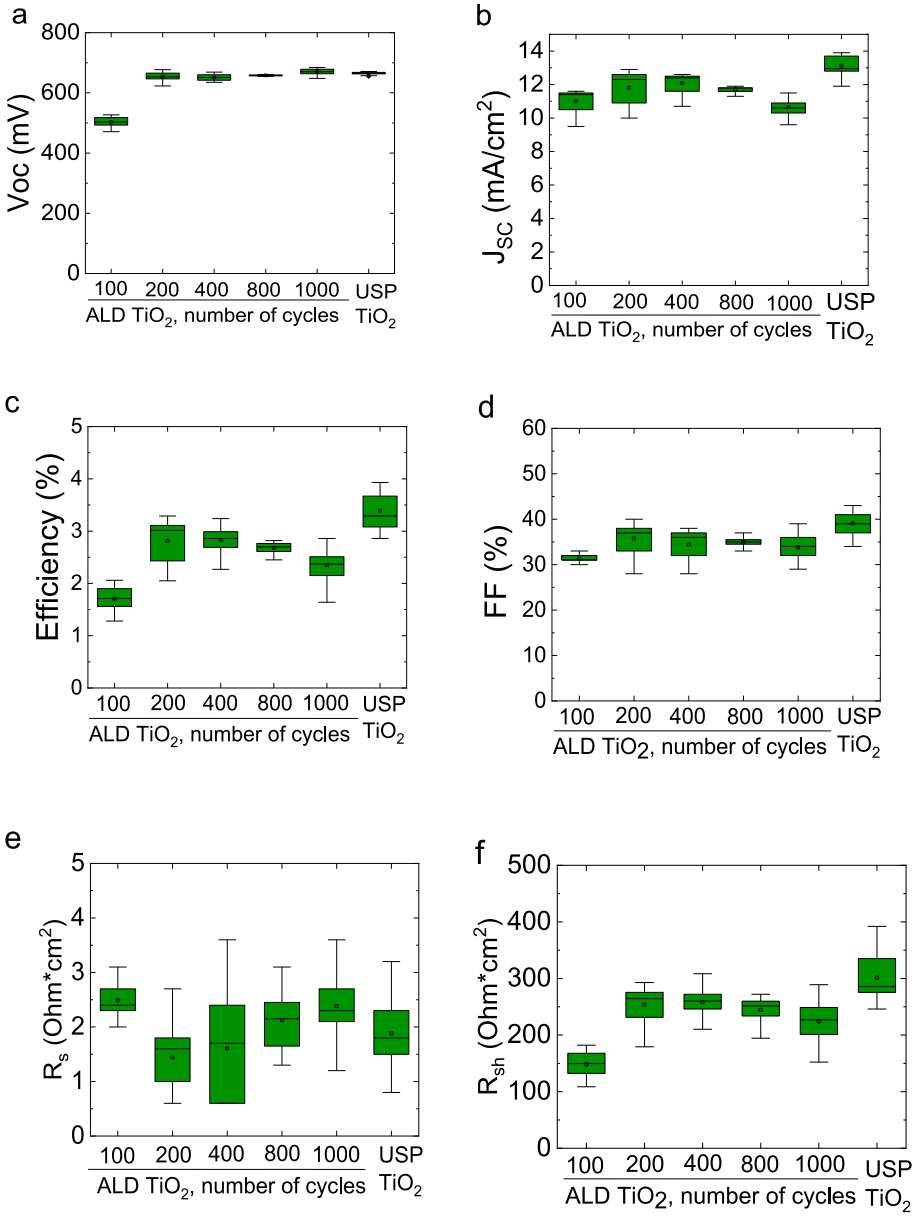

Fig. 4. Box plots of output parameters of SCs with ALD-TiO_2 deposited form 100, 200, 400, 800 and 1000 cycles and USP TiO_2 (70 spraying cycles) a) V_{OC}, b) j_{SC}, c) Efficiency, d) FF, e) R_S, f) R_{Sh}. The TiO_2 film thickness in solar cell devices fabricated by ALD using 400 cycles is ca. 30 nm and by USP is ca. 35–40 nm.

Table 1
Output parameters of SCs with ALD of various thicknesses and USP -TiO_2 (ca. 35–40 nm thickness). * 503 ± 17 - average + stand. deviation values, (521) – maximum value.

TiO_2 in SC structure	V_{OC}, mV	J_{SC}, mA cm^{-2}	FF, %	Efficiency, %	R_s, Ωcm^2	R_{sh}, Ωcm^2	Meas. cells
100 cycles ALD- TiO_2	503 ± 17(521)*	11.0 ± 0.7 (11.6)	31 ± 0.9 (33)	1.7 ± 0.2 (1.9)	2.5 ± 0.3 (3.1)	148 ± 25 (182)	13
200 cycles ALD- TiO_2	654 ± 13 (667)	11.8 ± 0.9 (12.9)	36 ± 3.3 (40)	2.8 ± 0.4 (3.3)	1.4 ± 0.5 (2.7)	254 ± 31 (293)	15
400 cycles ALD- TiO_2	651 ± 11 (662)	12.1 ± 0.5 (12.6)	34 ± 3.0 (37)	2.8 ± 0.2 (3.2)	1.6 ± 1.0 (3.6)	258 ± 22 (308)	12
800 cycles ALD- TiO_2	658 ± 8 (666)	11.7 ± 0.2 (11.9)	35 ± 1.2 (37)	2.7 ± 0.1 (2.8)	2.1 ± 0.6 (3.1)	244 ± 23 (272)	13
1000 cycles ALD -TiO_2	670 ± 11 (684)	10.7 ± 0.6 (11.9)	33 ± 2.2 (36)	2.4 ± 0.3 (2.7)	2.5 ± 0.5 (3.6)	224 ± 33 (289)	14
USP -TiO_2	665 ± 4 (670)	11.0 ± 2.1 (12.5)	39 ± 2.6 (43)	3.4 ± 0.3 (3.7)	1.9 ± 0.6 (3.2)	301 ± 41 (392)	16

and R_{Sh}, as observed in Fig. 4a and f, may suggest the ALD-TiO_2 film is too thin to provide complete coverage, potentially leading to increased shunting. Films ranging from 200 to 800 deposition cycles (15–50 nm) yield higher Voc values (~650 mV), as seen in Fig. 4a, which are comparable to the optimized Sb_2S_3 device employing USP-TiO_2. Increase can also be noted for J_{SC} and FF values for films deposited at 200–600 cycles, as observed in Fig. 4b and d, resulting in efficiencies around 3 %. However, thicker ALD-TiO_2 films (800 cycles and above, >60 nm) exhibit reduced J_{SC} values (~11 mA/cm^2) and FF (~33 %), thereby lowering solar cell PCE to 2–2.5 %. Optimal output parameters are achieved with ALD-ETL layers corresponding to 400 ALD deposition cycles (or approximately 30 nm thickness), yielding the highest SC performance (maximum PCE of approximately 3.3 %). The thickness of 30 nm appears to offer best balance between the series resistance and coverage for good p-n junction formation, evidenced by high V_{OC} and R_{Sh} values.

Previous studies have suggested varying optimal thicknesses for TiO_2 ETL layers in perovskite-type solar cell structures. Furthermore, ultrathin TiO_2 ETL-s have been proposed for various device architectures. Moerman et al. reported that thicknesses of 3–5 nm yielded the best output parameters, resulting in a PCE of 3.7 %, while a 10 nm ALD TiO_2 film resulted in a 1.2 % solar cell efficiency for an organic photovoltaic (OPV) device with structure ITO/TiO_2/OPV/PEDOT/MoO_3/Ag [38]. Zardetto et al. has reported that ALD-TiO_2 thickness of 2.75 nm is not enough to supress interfacial recombination, the TiO_2 thicknesses of 5.5–45 nm were found to be optimal thicknesses to provide sufficient blocking behaviour with overall PCE of the device of 6-6,3 % [39]. Shalan et al. reported the optimum thickness of ALD-TiO_2 film of 200 nm for perovskite based solar cell [36]. Thus, our results are in a good correspondence with many other studies on ALD-TiO_2 in perovskite type solar cells [36–39] indicating that TiO_2 thickness is an important factor for solar cell efficiency and should be optimized for a certain type of solar cell. These examples further emphasize the need to determine the optimal thickness for TiO_2 ETL, which is fundamental for designing a high performance Sb_2S_3 solar cell device.

The various thicknesses of USP-TiO_2 have already been studied by our group previously and in present study we rely on long-term established, optimized for this type solar cells and already several times published USP-TiO_2 thickness of 35–40 nm [2,3,6] which is comparable to ca. 30 nm thickness of USP-TiO_2. Thus, our comparative study confirms that for the SC with spray deposited Sb_2S_3 the TiO_2 layer thickness in the range of 30–40 nm independent of the TiO_2 deposition method (ALD, USP) seems to be optimal.

3.4. Electronic parameters and band alignment of solar cell

To understand the current transport mechanism and possible losses in the FTO/TiO_2/Sb_2S_3/P3HT/Au solar cells with USP and ALD-TiO_2 ETL layers, the KP and PYS measurements were performed for revealing the electronic parameters of all the constituent films and plotting the energy band diagrams. Thus, the absolute values of the work function (Φ) and ionization energies (E_i), which define the Fermi level (E_F) and the valence band maximum (E_{VBM}) positions with respect to the local vacuum level, were determined from KP and PYS measurements, respectively. The conduction band minimum (E_{CBM}) was calculated as $E_{CBM} = E_{VBM} + E_g$ by using the bandgaps of the respective films [49, 51–54,60–63]. E_{CBM} determined relative to the vacuum level defines the electron affinity (*EA*).

A similar ionization energy of 6.86 eV was found for both ALD-TiO_2 and USP-TiO_2 (see Table 2) indicating an identical surface chemistry. The work functions, however, show essential differences of about 130 meV changing from 4.05 eV for ALD-TiO_2 to 4.18 eV for USP-TiO_2 (see Fig. 5a). The electron affinities were calculated at 3.51 eV and 3.55 eV for ALD-TiO_2 and USP-TiO_2, respectively. We, thus, find the Fermi level in ALD-TiO_2 at 0.54 eV and in USP-TiO_2 at 0.64 eV below the conduction band minimum.

For the Sb_2S_3 films, the KP and PYS measurements reveal identical electronic properties irrespective of the deposition method used to grow TiO_2. According to considerations for the SPV in Experimental section, the recorded negative SPV of −0.277 V indicates the *n*-type conductivity of the as-deposited Sb_2S_3 layers on top of both TiO_2 films. Assuming flat band conditions achieved under illumination, we find for Sb_2S_3 the bulk values of $\Phi = 4.51$ eV and E_{CBM}-$E_F = 0.79$ eV. With the deposition of the P3HT hole transport layer the SPV of the device stack enhances significantly to −0.535 V demonstrating the development of the device V_{oc} (see Table 2). Note that the recorded negative SPV on the device stack points to collection of holes to the P3HT layer, which was expected. Not only the SPV values are identical for both devices with differently prepared TiO_2 layers but also the dynamics of charge carrier generation and separation under illumination are similar (see Fig. 5b). Minor differences are observed for charge carrier recombination dynamics. The recorded SPV values on devices completed by the Au back contact are slightly lower than those of the P3HT/Sb_2S_3/TiO_2/FTO/glass stack due to light intensity losses of the illumination passing through the semi-transparent gold layer with a thickness of about 10 nm. Otherwise, SPVs of the order of measured V_{oc}ś are expected.

With the known energy levels of all the films in the Au/P3HT/Sb_2S_3/TiO_2/FTO/glass solar cell device, we plot the energy band diagrams with respect to vacuum level alignment in Fig. 6a and relative to Fermi level in Fig. 6b. The diagrams bring in evidence the similarities and differences between electronic properties of the solar cells with the USP-TiO_2 and ALD-TiO_2 ETLs. Although the bulk CBM positions of Sb_2S_3 layers in Fig. 6a and b are almost identical, the different E_A data of the USP-TiO_2 and ALD-TiO_2 layers in Fig. 6a indicate on the existence of different CBM spikes at the TiO_2/Sb_2S_3 interface as a function of TiO_2 preparation method. We thus calculate a $\Delta E_{CBM} = EA_{Sb2S3} - EA_{TiO2}$ of 0.18 eV for USP-TiO_2 and 0.22 eV for ALD-TiO_2. Lower CBM spike at the USP-TiO_2/Sb_2S_3 interface would indicate an inferior recombination rate compared to that at the ALD-TiO_2/Sb_2S_3 interface. The mechanism of CBM spike formation at the ETL-absorber interface has been explained and widely accepted for CIS and Sb_2Se_3 chalcogenide-based devices. For a small CBM spike of ≤0.2 eV the thermionic emission across the junction would still allow unimpeded charge transport, whereas for a CBM spike ≥0.2 eV the electrostatic barrier to electrons is high enough impacting the efficient charge transfer at the main interface [65]. In addition, further differences in current transport through investigated devices may result from the large difference in the TiO_2 doping. Compared to the Fermi level of the ALD-TiO_2, the Fermi level in USP-TiO_2 is by about 100 meV deeper in the band gap with respect to CBM. As calculated in Table 2 and shown in Fig. 6b, the E_{CBM}-E_F is of 0.64 eV and 0.54 eV for the USP-TiO_2

Table 2
Electronic parameters of the SC component layers: band gap (Eg), surface photovoltage (SPV), work function (Φ), ionization energy (E_i), electron affinity (EA), valence band maximum with respect to Fermi level (E_F - E_{VBM}) and conduction band minimum relative to Fermi level (E_{CBM} - E_F).

Sample	Top layer Eg (eV)	SPV (±0.003 V)	Φ (±0.04 eV)		E_i (±0.03 eV)	E_A (±0.03 eV)	E_F - E_{VBM} (±0.05 eV)		E_{CBM} - E_F (±0.05 eV)	
			dark	light			dark	light	dark	light
FTO_lit [64].	4.10	–	4.60	4.60	8.70	4.60	–	–	–	–
ALD-TiO_2/FTO/glass	3.35	0	4.05	4.05	6.86	3.51	−2.81	−2.81	0.54	0.54
USP-TiO_2/FTO/glass	3.31	0	4.18	4.18	6.86	3.55	−2.67	−2.67	0.64	0.64
Sb_2S_3/ALD-TiO_2/FTO/glass	1.70	−0.277	4.79	4.51	5.43	3.73	−0.64	−0.91	1.07	0.79
P3HT/Sb_2S_3/ALD-TiO_2/FTO/glass	1.90	−0.535	4.70	4.17	4.84	2.94	−0.14	−0.67	1.76	1.23
Au/P3HT/Sb_2S_3/ALD-TiO_2/FTO/glass	–	−0.491	4.74	4.25	4.74	5.67	–	−0.49	–	–

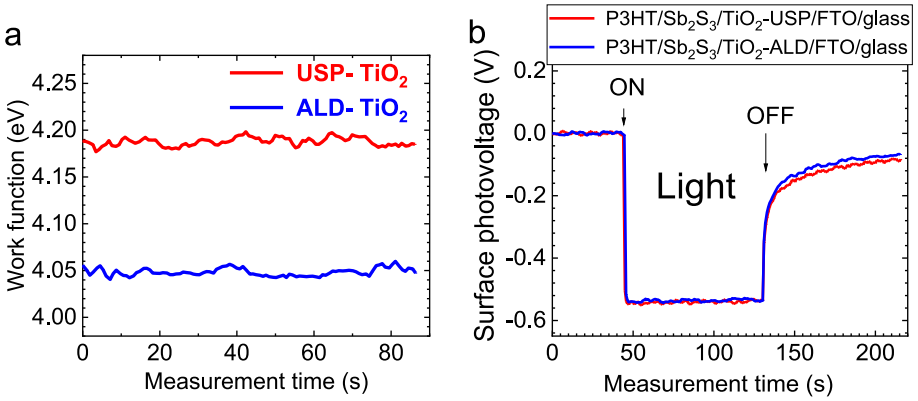

Fig. 5. a) Work function of the USP and ALD-TiO_2 thin films. b) Surface photovoltage of the SC stack with USP (red) and ALD (blue) TiO_2 ETL layers.

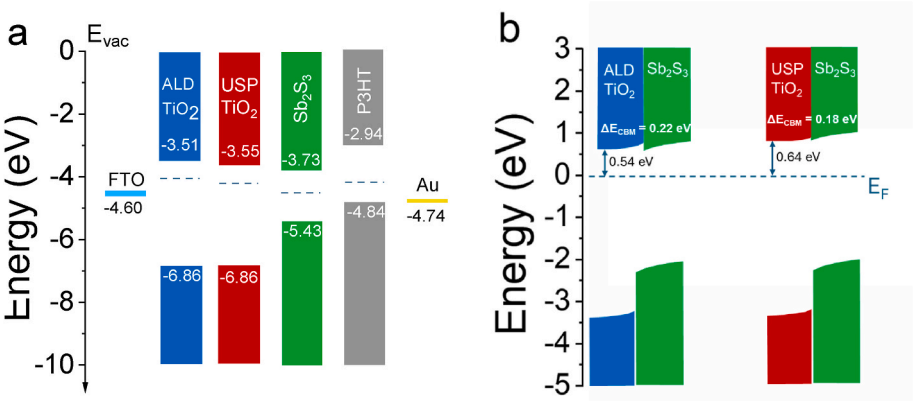

Fig. 6. a) SC energy level diagrams with ALD (blue box) and USP (red box) TiO_2 ETLs relative to vacuum energy level (E_{vac}). b) Band alignment when Fermi levels of ETL layers are aligned with that of Sb_2S_3. Valence band maximum (E_{VBM}) and conduction band minimum (E_{CBM}) values were calculated based on the work function measured under illuminated conditions.

and ALD-TiO_2, respectively. This points to a lower charge carrier concentration in USP-TiO_2 by approximately two orders of magnitude which will, consequently, largely extend the space charge region in the TiO_2 film for a better charge separation. The higher resistivity of the USP-TiO_2 films shall also have a positive impact on curing the possible pinholes between the front and back contacts of the devices. Thus, a higher shunt resistance is expected for devices with USP-TiO_2. This observation agrees with the measured electrical parameters of the solar cells shown in Table 1. Higher shunt resistances have also a beneficial effect on the device *FF* and V_{oc}, and as a result, on the solar cell efficiency. Therefore, higher efficiencies recorded on solar cells with USP-TiO_2 are explained by the reduced recombination at the TiO_2/Sb_2S_3 interface and enhanced parallel resistance.

At this point, it is worth mentioning that there are relatively few studies reporting the impact of ALD and USP-TiO_2 processing conditions on Sb_2S_3 solar cell performance. For instance, Pawar et al. [66] compared two device structures comprising ALD-SnO_2/CdS and ALD--TiO_2/CdS as double ETL layers. They demonstrated PCEs of 3.98 % and 4.23 % for the ALD-SnO_2/CdS and ALD-TiO_2/CdS based devices, respectively. The enhanced PCEs were mainly attributed to improved charge carrier collection and suitable band offset formation between the absorber and double ETLs. In a different approach, Kim et al. [67] employed a 70 nm thick sprayed TiO_2 ETL in an ALD-processed Sb_2S_3 absorber, following a device structure of Au/Poly-3-hexylthiophene/ALD-Sb_2S_3/bl-TiO_2/FTO, with a PCE of 5.77 %. However, their focus was on optimizing the ALD Sb_2S_3 absorber rather than the sprayed TiO_2, thus, these results cannot be directly compared.

4. Conclusions

We presented a comparative study of TiO_2 ETL layers synthesized by ultrasonic spray pyrolysis (USP) and atomic layer deposition (ALD) methods for Sb_2S_3 solar cells. Both USP and ALD methods led to the formation of TiO_2 thin films in the crystalline anatase phase. Texture analysis suggested that ALD-TiO_2 could enhance the growth of Sb_2S_3 crystals with favorable (hk1) crystal planes. Solar cell characterization revealed that the performance of ALD-TiO_2/Sb_2S_3 is highly dependent on the thickness of TiO_2 layer. Our comparative study confirms that for the SC with spray deposited Sb_2S_3 the optimal ETL TiO_2 layer thickness is in the range of 30–40 nm independent of the TiO_2 deposition method (ALD, USP). A layer that is too thin, at 100 deposition cycles or 5 nm, does not sufficiently suppress shunting, whereas thicker ALD TiO_2 films at deposition cycles of 800 cycles and above (thicknesses larger than 60 nm) increase series resistance, resulting in lower current yields. The optimal thickness for ALD-TiO_2, resulting in the highest output parameters, corresponds to 400 deposition cycles or approximately 30 nm, yielding a maximum PCE of around 3.3 %. Nevertheless, we found that the output parameters of solar cells with USP-TiO_2 are approximately 15 % higher than those of the best-performing ALD-TiO_2 samples. The average values of $V_{OC,}$ Jsc, FF, and PCE for USP-TiO_2 solar cells are 665 mV, 11.0 mA/cm^2, 39 %, and 3.4 %, respectively, compared to 651 mV, 12.1 mA/cm^2, 34 %, and 2.8 % for ALD-TiO_2 solar cells. Photoelectron yield spectroscopy (PYS) and Kelvin probe (KP) measurements facilitated the construction of electronic band diagrams, revealing a lower doping of the USP-TiO_2 layers and a smaller conduction band minimum spike at the USP-TiO_2/Sb_2S_3 interface. The lower CBM spike at the USP-TiO_2/Sb_2S_3 interface indicates a reduced recombination rate compared to that at the ALD-TiO_2/Sb_2S_3 interface. In conjunction with an adjusted doping, this could explain the higher efficiencies observed with USP-TiO_2. While ALD is known for highly reproducible, uniform, pinhole-free growth of thin films, our findings highlight the suitability of USP-TiO_2, offering cost-effective advantages over ALD and enabling the production of high-quality electron transport layers for thin film Sb_2S_3 solar cells.

CRediT authorship contribution statement

T. Dedova: Writing – review & editing, Writing – original draft, Methodology, Investigation, Data curation. **R. Krautmann:** Writing – review & editing, Formal analysis, Data curation. **M. Rusu:** Writing – review & editing, Validation, Methodology, Formal analysis, Data curation. **A. Katerski:** Software, Methodology, Formal analysis. **M. Krunks:** Writing – review & editing, Funding acquisition, Data curation, Conceptualization. **T. Unold:** Writing – review & editing, Validation, Methodology, Formal analysis. **N. Spalatu:** Writing – review & editing, Visualization, Data curation. **A. Mere:** Methodology, Formal analysis, Data curation. **J. Sydorenko:** Writing – review & editing, Formal analysis, Data curation. **M. Sibiński:** Writing – review & editing, Formal analysis. **I. Oja Acik:** Writing – review & editing, Validation, Supervision, Project administration, Funding acquisition, Conceptualization.

5. Artificial intelligence

The authors claim that no AI was used in any step of manuscript preparation, neither for the study conceptualisation nor for writing process.

Declaration of competing interest

The authors declare that they have no known competing financial interests or personal relationships that could have appeared to influence the work reported in this paper.

Acknowledgements

This study was funded by the Estonian Research Council project PRG627, “Antimony Chalcogenide thin films for next-generation semi-transparent solar cells applicable in electricity producing windows”, the Estonian Ministry of Education and Research project TK210; TK210U8 “Center of Excellence in Sustainable Green Hydrogen and Energy Technologies”, and the work supported by EU Horizon 2020 project 952509-5GSOLAR.

This research was funded by CETPartnership, the Clean Energy Transition Partnership under the 2022 CETPartnership joint call for research proposals, co-funded by the European Commission (GA N°101069750), and with the funding organisation Estonian Research Council, agreement No MOB3PRT2.

The article is based upon work from COST Action Research and International Networking on Emerging Inorganic Chalcogenides for Photovoltaics (RENEW-PV), CA21148, supported by COST (European Cooperation in Science and Technology).

The research was conducted using the NAMUR + core facility funded by projects “Center of nanomaterials technologies and research” (2014-2020.4.01.16-0123) and TT13.

Dr. Olga Volobujeva is thanked for SEM images.

Appendix A. Supplementary data

Supplementary data to this article can be found online at https://doi.org/10.1016/j.solmat.2024.113279.

Data availability

The data that support the findings of this study are available on request from the corresponding author (T. Dedova).

References

[1] J. Han, X. Pu, H. Zhou, Q. Cao, S. Wang, Z. He, B. Gao, T. Li, J. Zhao, X. Li, Synergistic effect through the introduction of inorganic zinc halides at the interface of TiO 2 and Sb 2 S 3 for high-performance Sb 2 S 3 planar thin-film solar cells, ACS Appl. Mater. Interfaces 12 (2020) 44297–44306, https://doi.org/10.1021/acsami.0c11550.

[2] S. Mandati, N. Juneja, A. Katerski, A. Jegorovė, R. Grzibovskis, A. Vembris, T. Dedova, N. Spalatu, A. Magomedov, S. Karazhanov, V. Getautis, M. Krunks, I. Oja Acik, 4.9% efficient Sb $_2$ S $_3$ solar cells from semitransparent absorbers with fluorene-based thiophene-terminated hole conductors, ACS Appl. Energy Mater. 6 (2023) 3822–3833, https://doi.org/10.1021/acsaem.2c04097.

[3] J.S. Eensalu, A. Katerski, E. Kärber, L. Weinhardt, M. Blum, C. Heske, W. Yang, I. Oja Acik, M. Krunks, Semitransparent Sb $_2$ S $_3$ thin film solar cells by ultrasonic spray pyrolysis for use in solar windows, Beilstein J. Nanotechnol. 10 (2019) 2396–2409, https://doi.org/10.3762/bjnano.10.230.

[4] R. Tang, X. Wang, C. Jiang, S. Li, G. Jiang, S. Yang, C. Zhu, T. Chen, Vacuum assisted solution processing for highly efficient Sb $_2$ S $_3$ solar cells, J. Mater. Chem. A 6 (2018) 16322–16327, https://doi.org/10.1039/C8TA05614E.

[5] H. Deng, Y. Zeng, M. Ishaq, S. Yuan, H. Zhang, X. Yang, M. Hou, U. Farooq, J. Huang, K. Sun, R. Webster, H. Wu, Z. Chen, F. Yi, H. Song, X. Hao, J. Tang, Quasiepitaxy strategy for efficient full-inorganic Sb $_2$ S $_3$ solar cells, Adv. Funct. Mater. 29 (2019), https://doi.org/10.1002/adfm.201901720.

[6] N. Juneja, S. Mandati, A. Katerski, N. Spalatu, S. Daskeviciute-Geguziene, A. Vembris, S. Karazhanov, V. Getautis, M. Krunks, I. Oja Acik, Sb $_2$ S $_3$ solar cells with a cost-effective and dopant-free fluorene-based enamine as a hole transport material, Sustain. Energy Fuels 6 (2022) 3220–3229, https://doi.org/10.1039/D2SE00356B.

[7] U.A. Shah, S. Chen, G.M.G. Khalaf, Z. Jin, H. Song, Wide bandgap Sb $_2$ S $_3$ solar cells, Adv. Funct. Mater. 31 (2021), https://doi.org/10.1002/adfm.202100265.

[8] Z. Li, X. Liang, G. Li, H. Liu, H. Zhang, J. Guo, J. Chen, K. Shen, X. San, W. Yu, R.E. I. Schropp, Y. Mai, 9.2%-efficient core-shell structured antimony selenide nanorod array solar cells, Nat. Commun. 10 (2019) 125, https://doi.org/10.1038/s41467-018-07903-6.

[9] L. Wang, D.-B. Li, K. Li, C. Chen, H.-X. Deng, L. Gao, Y. Zhao, F. Jiang, L. Li, F. Huang, Y. He, H. Song, G. Niu, J. Tang, Stable 6%-efficient Sb2Se3 solar cells with a ZnO buffer layer, Nat. Energy 2 (2017) 17046, https://doi.org/10.1038/nenergy.2017.46.

[10] Z. Duan, X. Liang, Y. Feng, H. Ma, B. Liang, Y. Wang, S. Luo, S. Wang, R.E. I. Schropp, Y. Mai, Z. Li, Sb $_2$ Se $_3$ thin-film solar cells exceeding 10% power conversion efficiency enabled by injection vapor deposition Technology, Adv. Mater. 34 (2022), https://doi.org/10.1002/adma.202202969.

[11] C. Chen, L. Wang, L. Gao, D. Nam, D. Li, K. Li, Y. Zhao, C. Ge, H. Cheong, H. Liu, H. Song, J. Tang, 6.5% certified efficiency Sb $_2$ Se $_3$ solar cells using PbS colloidal quantum dot film as hole-transporting layer, ACS Energy Lett. 2 (2017) 2125–2132, https://doi.org/10.1021/acsenergylett.7b00648.

[12] Y. Zhao, S. Wang, C. Jiang, C. Li, P. Xiao, R. Tang, J. Gong, G. Chen, T. Chen, J. Li, X. Xiao, Regulating energy band alignment via alkaline metal fluoride assisted solution post-treatment enabling Sb $_2$ (S,Se) $_3$ solar cells with 10.7% efficiency, Adv. Energy Mater. 12 (2022), https://doi.org/10.1002/aenm.202103015.

[13] C. Qian, K. Sun, J. Cong, H. Cai, J. Huang, C. Li, R. Cao, Z. Liu, M. Green, B. Hoex, T. Chen, X. Hao, Bifacial and semitransparent Sb $_2$ (S,Se) $_3$ solar cells for single-junction and tandem photovoltaic applications, Adv. Mater. 35 (2023), https://doi.org/10.1002/adma.202303936.

[14] R. Tang, X. Wang, W. Lian, J. Huang, Q. Wei, M. Huang, Y. Yin, C. Jiang, S. Yang, G. Xing, S. Chen, C. Zhu, X. Hao, M.A. Green, T. Chen, Hydrothermal deposition of antimony selenosulfide thin films enables solar cells with 10% efficiency, Nat. Energy 5 (2020) 587–595, https://doi.org/10.1038/s41560-020-0652-3.

[15] Z. Feng, S. Sun, Y. Sun, X. Liu, H. Liu, H. Liu, Efficient CdS buffered TiO2 electronic transport layer for Sb2S3 solar cells by a facile spinning coating process, Appl. Phys. A 128 (2022) 479, https://doi.org/10.1007/s00339-022-05627-5.

[16] N. Ali, R. Ahmed, B. ul Haq, A. Shaari, R. Hussain, S. Goumri-Said, A novel approach for the synthesis of tin antimony sulphide thin films for photovoltaic application, Sol. Energy 113 (2015) 25–33, https://doi.org/10.1016/j.solener.2014.12.021.

[17] C.-H. Cheng, M. Li, H.-Q. Song, W.-H. Li, J. Leng, W. Tian, R. Cui, C. Zhao, S. Jin, W. Liu, S. Cong, Enhanced performance of the Sb $_2$ Se $_3$ thin-film solar cell by organic molecule-induced crystallization and suppression of the interface recombination, ACS Appl. Energy Mater. 4 (2021) 5079–5085, https://doi.org/10.1021/acsaem.1c00640.

[18] A. Hayali, M.M. Alkaisi, High efficiency perovskite solar cells using DC sputtered compact TiO $_2$ electron transport layer, EPJ Photovoltaics 12 (2021) 8, https://doi.org/10.1051/epjpv/2021008.

[19] M. Shirazi, R. Sabet Dariani, M.R. Toroghinejad, Efficiency enhancement of hole-conductor-free perovskite solar cell based on ZnO nanostructure by Al doping in ZnO, J. Alloys Compd. 692 (2017) 492–502, https://doi.org/10.1016/j.jallcom.2016.09.038.

[20] X. Jin, Y. Fang, T. Salim, M. Feng, S. Hadke, S.W. Leow, T.C. Sum, L.H. Wong, In situ growth of [hk1]-Oriented Sb $_2$ S $_3$ for solution-processed planar heterojunction solar cell with 6.4% efficiency, Adv. Funct. Mater. 30 (2020), https://doi.org/10.1002/adfm.202002887.

[21] C.H. Don, T.P. Shalvey, M.J. Smiles, L. Thomas, L.J. Phillips, T.D.C. Hobson, H. Finch, L.A.H. Jones, J.E.N. Swallow, N. Fleck, C. Markwell, P.K. Thakur, T. Lee, D. Biswas, L. Bowen, B.A.D. Williamson, D.O. Scanlon, V.R. Dhanak, K. Durose, T. D. Veal, J.D. Major, Multi-phase sputtered TiO $_2$ -induced current–voltage distortion in Sb $_2$ Se $_3$ solar cells, Adv. Mater. Interfaces 10 (2023), https://doi.org/10.1002/admi.202300238.

[22] L. Guo, B. Zhang, S. Ranjit, J. Wall, S. Saurav, A.J. Hauser, G. Xing, L. Li, X. Qian, F. Yan, Interface engineering via sputtered oxygenated CdS:O window layer for highly efficient Sb $_2$ Se $_3$ thin-film solar cells with efficiency above 7, Sol. RRL 3 (2019), https://doi.org/10.1002/solr.201900225.

[23] L.J. Phillips, C.N. Savory, O.S. Hutter, P.J. Yates, H. Shiel, S. Mariotti, L. Bowen, M. Birkett, K. Durose, D.O. Scanlon, J.D. Major, Current enhancement via a TiO2 window layer for CSS Sb2Se3 solar cells: performance limits and high V_{oc}, IEEE J. Photovoltaics 9 (2019) 544–551, https://doi.org/10.1109/JPHOTOV.2018.2885836.

[24] Y.S. Kim, H.-J. Jin, H.R. Jung, J. Kim, B.P. Nguyen, J. Kim, W. Jo, Reduced extrinsic recombination process in anatase and rutile TiO2 epitaxial thin films for efficient electron transport layers, Sci. Rep. 11 (2021) 6810, https://doi.org/10.1038/s41598-021-86422-9.

[25] M. Bhogaita, S. Yadav, A.U. Bhanushali, A.A. Parsola, R. Pratibha Nalini, Synthesis and characterization of TiO2 thin films for DSSC prototype, Mater. Today Proc. 3 (2016) 2052–2061, https://doi.org/10.1016/j.matpr.2016.04.108.

[26] K. Li, C. Chen, S. Lu, C. Wang, S. Wang, Y. Lu, J. Tang, Orientation engineering in low-dimensional crystal-structural materials via seed screening, Adv. Mater. 31 (2019), https://doi.org/10.1002/adma.201903914.

[27] Y.C. Choi, D.U. Lee, J.H. Noh, E.K. Kim, S. Il Seok, Highly improved Sb $_2$ S $_3$ sensitized-inorganic–organic heterojunction solar cells and quantification of traps by deep-level transient spectroscopy, Adv. Funct. Mater. 24 (2014) 3587–3592, https://doi.org/10.1002/adfm.201304238.

[28] U.K. Thakur, A.M. Askar, R. Kisslinger, B.D. Wiltshire, P. Kar, K. Shankar, Halide perovskite solar cells using monocrystalline TiO $_2$ nanorod arrays as electron transport layers: impact of nanorod morphology, Nanotechnology 28 (2017) 274001, https://doi.org/10.1088/1361-6528/aa75ab.

[29] A. Hernández-Granados, A.N. Corpus-Mendoza, P.M. Moreno-Romero, C. A. Rodríguez-Castañeda, J.E. Pascoe-Sussoni, O.A. Castelo-González, E. C. Menchaca-Campos, J. Escorcia-García, H. Hu, Optically uniform thin films of mesoporous TiO2 for perovskite solar cell applications, Opt. Mater. 88 (2019) 695–703, https://doi.org/10.1016/j.optmat.2018.12.044.

[30] C. Byrne, R. Fagan, S. Hinder, D.E. McCormack, S.C. Pillai, New approach of modifying the anatase to rutile transition temperature in TiO $_2$ photocatalysts, RSC Adv. 6 (2016) 95232–95238, https://doi.org/10.1039/C6RA19759K.

[31] D.A.H. Hanaor, C.C. Sorrell, Review of the anatase to rutile phase transformation, J. Mater. Sci. 46 (2011) 855–874, https://doi.org/10.1007/s10853-010-5113-0.

[32] M.N. Chaudhari, Thin film deposition methods: a critical review, Int. J. Res. Appl. Sci. Eng. Technol. 9 (2021) 5215–5232, https://doi.org/10.22214/ijraset.2021.36154.

[33] I.-D. Simandan, F. Sava, A.-T. Buruiana, I. Burducea, N. Becherescu, C. Mihai, A. Velea, A.-C. Galca, The effect of the deposition method on the structural and optical properties of ZnS thin films, Coatings 11 (2021) 1064, https://doi.org/10.3390/coatings11091064.

[34] B.A. Al-Asbahi, S.M.H. Qaid, M. Hezam, I. Bedja, H.M. Ghaithan, A.S. Aldwayyan, Effect of deposition method on the structural and optical properties of CH3NH3PbI3 perovskite thin films, Opt. Mater. 103 (2020) 109836, https://doi.org/10.1016/j.optmat.2020.109836.

[35] R. Parize, T. Cossuet, O. Chaix-Pluchery, H. Roussel, E. Appert, V. Consonni, In situ analysis of the crystallization process of Sb 2 S 3 thin films by Raman scattering and X-ray diffraction, Mater. Des. 121 (2017) 1–10, https://doi.org/10.1016/j.matdes.2017.02.034.

[36] A.E. Shalan, S. Narra, T. Oshikiri, K. Ueno, X. Shi, H.-P. Wu, M.M. Elshanawany, E. Wei-Guang Diau, H. Misawa, Optimization of a compact layer of TiO $_2$ via atomic-layer deposition for high-performance perovskite solar cells, Sustain. Energy Fuels 1 (2017) 1533–1540, https://doi.org/10.1039/C7SE00220C.

[37] C.-H. Hsu, K.-T. Chen, L.-S. Liang, P. Gao, S.-L. Ou, W.-Y. Wu, P.-H. Huang, S.-Y. Lien, Improved perovskite solar cell performance by high growth rate spatial atomic layer deposited titanium oxide compact layer, IEEE J. Electron Devices Soc. 9 (2021) 49–56, https://doi.org/10.1109/JEDS.2020.3039189.

[38] D. Moerman, H. Kim, A.E. Colbert, S. Graham, D.S. Ginger, The impact of ultra-thin titania interlayers on open circuit voltage and carrier lifetime in thin film solar cells, Appl. Phys. Lett. 108 (2016), https://doi.org/10.1063/1.4944049.

[39] V. Zardetto, F. Di Giacomo, G. Lucarelli, W.M.M. Kessels, T.M. Brown, M. Creatore, Plasma-assisted atomic layer deposition of TiO2 compact layers for flexible mesostructured perovskite solar cells, Sol. Energy 150 (2017) 447–453, https://doi.org/10.1016/j.solener.2017.04.028.

[40] R. Parize, A. Katerski, I. Gromyko, L. Rapenne, H. Roussel, E. Kärber, E. Appert, M. Krunks, V. Consonni, ZnO/TiO $_2$/Sb $_2$ S $_3$ core–shell nanowire heterostructure for extremely thin absorber solar cells, J. Phys. Chem. C 121 (2017) 9672–9680, https://doi.org/10.1021/acs.jpcc.7b00178.

[41] W. Zhu, Z. Zhang, W. Chai, Q. Zhang, D. Chen, Z. Lin, J. Chang, J. Zhang, C. Zhang, Y. Hao, Band alignment engineering towards high efficiency carbon-based inorganic planar CsPbIBr $_2$ perovskite solar cells, ChemSusChem 12 (2019) 2318–2325, https://doi.org/10.1002/cssc.201900611.

[42] R.W. Johnson, A. Hultqvist, S.F. Bent, A brief review of atomic layer deposition: from fundamentals to applications, Mater, Today Off. 17 (2014) 236–246, https://doi.org/10.1016/j.mattod.2014.04.026.

[43] M. Leskelä, M. Mattinen, M. Ritala, Review Article: atomic layer deposition of optoelectronic materials, J. Vac. Sci. Technol. B, Nanotechnol. Microelectron. Mater. Process. Meas. Phenom. 37 (2019), https://doi.org/10.1116/1.5083692.

[44] W. Niu, X. Li, S.K. Karuturi, D.W. Fam, H. Fan, S. Shrestha, L.H. Wong, A.I.Y. Tok, Applications of atomic layer deposition in solar cells, Nanotechnology 26 (2015) 064001, https://doi.org/10.1088/0957-4484/26/6/064001.

[45] A.B. Workie, H.S. Ningsih, S.-J. Shih, An comprehensive review on the spray pyrolysis technique: historical context, operational factors, classifications, and product applications, J. Anal. Appl. Pyrolysis 170 (2023) 105915, https://doi.org/10.1016/j.jaap.2023.105915.

[46] D.K. Schroder, Semiconductor Material and Device Characterisation, John Willey & Sohns, Inc., New York/Chichester/Brisbane/Toronto/Singapore, 1990.

[47] L. Haryński, A. Olejnik, K. Grochowska, K. Siuzdak, A facile method for Tauc exponent and corresponding electronic transitions determination in semiconductors directly from UV–Vis spectroscopy data, Opt. Mater. 127 (2022) 112205, https://doi.org/10.1016/j.optmat.2022.112205.

[48] P. Makula, M. Pacia, W. Macyk, How to correctly determine the band gap energy of modified semiconductor photocatalysts based on UV–vis spectra, J. Phys. Chem. Lett. 9 (2018) 6814–6817, https://doi.org/10.1021/acs.jpclett.8b02892.

[49] M. Rusu, T. Kodalle, L. Choubrac, N. Barreau, C.A. Kaufmann, R. Schlatmann, T. Unold, Electronic structure of the CdS/Cu(in,Ga)Se 2 interface of KF- and RbF-treated samples by Kelvin probe and photoelectron yield spectroscopy, ACS Appl. Mater. Interfaces 13 (2021) 7745–7755, https://doi.org/10.1021/acsami.0c20976.

[50] RUFF Database, 2019. Http//Rruff.Info/Anatase/R060277. (Accessed 8 October 2019).

[51] J. Spiridonova, A. Katerski, M. Danilson, M. Krichevskaya, M. Krunks, I. Oja Acik, Effect of the titanium isopropoxide:acetylacetone molar ratio on the photocatalytic activity of TiO2 thin films, Molecules 24 (2019) 4326, https://doi.org/10.3390/molecules24234326.

[52] J. Spiridonova, A. Mere, M. Krunks, M. Rosenberg, A. Kahru, M. Danilson, M. Krichevskaya, I. Oja Acik, Enhanced visible and ultraviolet light-induced gas-phase photocatalytic activity of TiO2 thin films modified by increased amount of acetylacetone in precursor solution for spray pyrolysis, Catalysts 10 (2020) 1011, https://doi.org/10.3390/catal10091011.

[53] A. Jolivet, C. Labbé, C. Frilay, O. Debieu, P. Marie, B. Horcholle, F. Lemarié, X. Portier, C. Grygiel, S. Duprey, W. Jadwisienczak, D. Ingram, M. Upadhyay, A. David, A. Fouchet, U. Lüders, J. Cardin, Structural, optical, and electrical properties of TiO2 thin films deposited by ALD: impact of the substrate, the deposited thickness and the deposition temperature, Appl. Surf. Sci. 608 (2023) 155214, https://doi.org/10.1016/j.apsusc.2022.155214.

[54] H.K. Chung, S.O. Won, Y. Park, J.-S. Kim, T.J. Park, S.K. Kim, Atomic-layer deposition of TiO2 thin films with a thermally stable (CpMe5)Ti(OMe)3 precursor, Appl. Surf. Sci. 550 (2021) 149381, https://doi.org/10.1016/j.apsusc.2021.149381.

[55] J. Zhang, P. Zhou, J. Liu, J. Yu, New understanding of the difference of photocatalytic activity among anatase, rutile and brookite TiO_2, Phys. Chem. Chem. Phys. 16 (2014) 20382, https://doi.org/10.1039/C4CP02201G.

[56] S.H. Park, A. Katoch, K.H. Chae, S. Gautam, P. Miedema, S.W. Cho, M. Kim, R.-P. Wang, M. Lazemi, F. Groot, S. Kwon, Direct and real-time observation of hole transport dynamics in anatase TiO2 using X-ray free-electron laser, Nat. Commun. 13 (2022) 2531, https://doi.org/10.1038/s41467-022-30336-1.
[57] J.I. Pankove, Optical Processes in Semiconductors, Dover Publications, 2012.
[58] H. Zhong, F. Pan, S. Yue, C. Qin, V. Hadjiev, F. Tian, X. Liu, F. Lin, Z. Wang, J. Bao, Idealizing Tauc plot for accurate bandgap determination of semiconductor with ultraviolet–visible spectroscopy: a case study for cubic boron arsenide, The Journal of Physical Chemistry Letters, J. Phys. Chem. Lett. 14 (2023) 6702–6708, https://doi.org/10.1021/acs.jpclett.3c01416.
[59] R. Corkish, M.A. Green, Band edge optical absorption in intrinsic silicon: assessment of the indirect transition and disorder models, J. Appl. Phys. 73 (1993) 3988, https://doi.org/10.1063/1.352864.
[60] Y.J. Shi, R.J. Zhang, H. Zheng, D.H. Li, W. Wei, X. Chen, Y. Sun, Y.F. Wei, H.L. Lu, N. Dai, L.Y. Chen, Optical constants and band gap evolution with phase transition in sub-20-nm-thick TiO2 films prepared by ALD, Nanoscale Res. Lett. 12 (2017) 243, https://doi.org/10.1186/s11671-017-2011-2.
[61] T. Luttrell, S. Halpegamage, J. Tao, A. Kramer, E. Sutter, M. Batzill, Why is anatase a better photocatalyst than rutile? - model studies on epitaxial TiO2 films, Sci. Rep. 4 (2014) 4043, https://doi.org/10.1038/srep04043.
[62] T. Dittrich, J. Sydorenko, N. Spalatu, N.H. Nickel, A. Mere, M. Krunks, I. Oja Acik, Synthesis control of charge separation at anatase TiO_2 thin films studied by transient surface photovoltage spectroscopy, ACS Appl. Mater. Interfaces 14 (2022) 1944–8244, https://doi.org/10.1021/acsami.2c09032.
[63] W. Zhu, Z. Zhang, W. Chai, Q. Zhang, D. Chen, Z. Lin, J. Chang, J. Zhang, C. Zhang, Y. Hao, Band alignment engineering towards high efficiency carbon-based inorganic planar CsPbIBr 2 perovskite solar cells, ChemSusChem 12 (2019) 2318–2325, https://doi.org/10.1002/cssc.201900611.
[64] B. Stjerna, E. Olsson, C.G. Granqvist, Optical and electrical properties of radio frequency sputtered tin oxide films doped with oxygen vacancies, F, Sb, or Mo, J. Appl. Phys. 76 (1994) 3797–3817, https://doi.org/10.1063/1.357383.
[65] H. Shiel, O. Hutter, L. Phillips, J. Swallow, L. Jones, T. Featherstone, M. Smiles, P. Thakur, T. Lee, V. Dhanak, J. Major, T. Veal, Natural band alignments and band offsets of Sb_2Se_3 solar cells, ACS Appl. Energy Mater. 3 (2020) 11617–11626, https://doi.org/10.1021/acsaem.0c01477.
[66] P.S. Pawar, R. Nandi, K.R.E. Neerugatti, I. Sharma, R.K. Yadav, Y.T. Kim, J. Cho, J. Heo, Atomic-layer-deposited TiO2 and SnO2 coupled with CdS as double buffer layers for HTL-free Sb2S3 thin-film solar cells, Sol. Energy 246 (2022) 141–151, https://doi.org/10.1016/j.solener.2022.09.044.
[67] K. Kim, S.J. Lee, M. Park, J.-K. Kang, J.H. Heo, S.H. Im, S.-J. Sung, Highly reproducible planar Sb2S3-sensitized solar cells based on atomic layer deposition, Nanoscale 6 (2014) 14549–14554, https://doi.org/10.1039/C4NR04148H.